

Article pubs.acs.org/crystal

# Elaborate Supramolecular Architectures Formed by Co-Assembly of **Metal Species and Peptoid Macrocycles**

Linhai Jiang, Chunhua Tony Hu, Francesco De Riccardis, and Kent Kirshenbaum\*



Cite This: Cryst. Growth Des. 2021, 21, 3889-3901



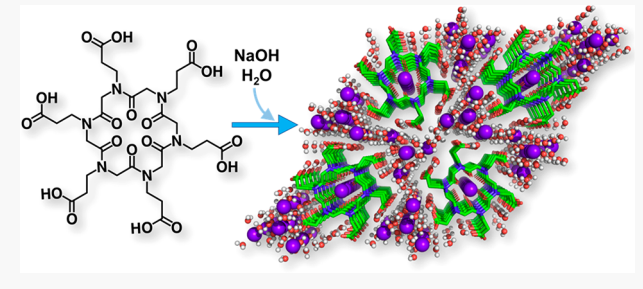
**ACCESS** I

III Metrics & More

Article Recommendations

Supporting Information

ABSTRACT: Peptoids are a family of sequence-specific oligomers capable of mimicking the structure and function of polypeptides. The innate folding and self-assembly capabilities of peptoid oligomers can be enhanced by the presence of coordinated metal ions. In this work, we explore the co-assembly of water-soluble hexameric and tetrameric peptoid macrocycles with Na<sup>+</sup> and K<sup>+</sup> ions. Solid-state structures were solved for six cyclopeptoid-metal coassemblies by X-ray diffraction using single crystals grown from fully aqueous solutions. Subtle variations in the peptoid oligomer composition give rise to dramatic alterations in the supramolecular assemblies. Some



structures feature extensively hydrated porous architectures that include unusual metal ion clusters. The ability to study the metallopeptoid structure at an atomic resolution in crystals obtained from an aqueous solution is an important advancement, as most previous peptoid crystal structures were obtained from nonaqueous or cosolvent solutions. These results will facilitate the design of peptoids and other foldamers for the assembly of supramolecular frameworks.

## ■ INTRODUCTION

Oligomers of N-substituted glycine units are known as peptoids and constitute an important family of synthetic peptidomimetic oligomers. 1-6 Over the past two decades, peptoids have garnered attention as a platform for the discovery of functional molecules due to their capacity to mimic bioactive peptides. 7-20 Peptoids notably differ from their  $\alpha$ -peptide counterparts because of the presence of tertiary amide linkages between the monomer units. This feature endows peptoids with an exceptional resistance to proteolytic degradation. The absence of hydrogen bonding and the facile conformational interconversions between cisand trans-amide conformations can preclude long-range structural ordering for peptoid oligomers. However, the strategic incorporation of particular side chain types, the ingenious formation of long-range interactions between functional groups, and macrocyclization allow researchers to obtain stable structural motifs. Peptoid secondary structures now include polyproline type-I and type-II helices,  $^{21-28}$  a "threaded-loop" conformation,  $^{29}$  peptoid ribbons,  $^{30,31}$  a square-shaped  $\eta$ -helix,  $^{32}$   $\omega$ -strands,  $^{33}$   $\Sigma$ -strands,  $^{34}$  and turn or loop structures.  $^{35-37}$ or loop structures.35

One particularly attractive strategy to enforce peptoid folding has been the addition of extrinsic chemical species, such as metal ions, that are capable of a specific association with the peptoid backbone or side chain functional groups. Similar to metallopeptides and metalloproteins,<sup>38</sup> resultant assemblies can populate unusual conformations that otherwise may not be energetically favored. Pioneering work from the Zuckermann group suggested that zinc-

mediated side chain interactions may direct the folding of helical peptoids into a two-helix bundle. 44 The Maayan group has extensively explored the capability of linear peptoids bearing specific side chain functional groups to coordinate with transition metal ions. 45-50 Using this strategy, both intramolecular and intermolecular side chain to metal interactions were established, leading to the ordering of linear peptoid oligomers and their supramolecular organization within the crystal lattice.  $^{48,51,52}$  Interactions between backbone amide groups of macrocyclic peptoids and metal cations have also been a focus of the De Riccardis and Izzo group. In addition to controlling the backbone conformation of peptoid macrocycles, the De Riccardis and Izzo group highlighted the potential applications of metal-binding cyclopeptoids, such as ion sequestration and phase-transfer catalysis. 24,35,53-55 Indeed, peptoids can be regarded as an optimal molecular platform for the design of multidentate metal ligands due to the modular nature of peptoid synthesis and the ability to incorporate chemically diverse side chain groups, including sites for metal coordination, at specified positions along the oligomer sequence. 56-61 Important advances have also been made in directing peptoid self-

Received: February 22, 2021 Revised: April 26, 2021 Published: May 18, 2021





assembly to create supramolecular assemblies, such as two-dimensional nanosheets, that can be readily modified to address an array of materials applications.  $^{62-64}$ 

Herein, we consider whether the well-known structural attributes of peptoid macrocycles<sup>35,65–68</sup> and the concurrent presence of chelating side chain carboxyl and backbone amide carbonyl groups can give rise to novel metalated supramolecular architectures. We compare the backbone conformations, the crystal packing forces, and the metal coordination modes of hexamer and tetramer peptoid macrocycles that incorporate different carboxylate side chains in the presence of Na<sup>+</sup> or K<sup>+</sup> cations. We report here the X-ray crystal structures of several such peptoid—metal coassemblies as obtained from crystals grown in fully aqueous conditions. We observed extraordinary and unanticipated framework architectures in the crystal lattices, providing a notable advancement in the development of supramolecular peptoid assemblies.

# RESULTS

**Peptoid Design and Synthesis.** A series of macrocyclic peptoid oligomers, including two hexamers and four tetramers, were designed, synthesized, and characterized in this work. The cyclopeptoids included a carboxylic acid functional group in each of the side chains. The linear precursors were synthesized using the "submonomer" solid-phase synthesis protocols introduced by Zuckermann. Three protected amine submonomers (*tert*-butyl aminoacetate, *tert*-butyl 3-aminopropanoate, and *tert*-butyl 4-aminobutyrate) were used as synthons to alter the lengths of the alkyl groups within the monomer side chains (Scheme 1A—C).

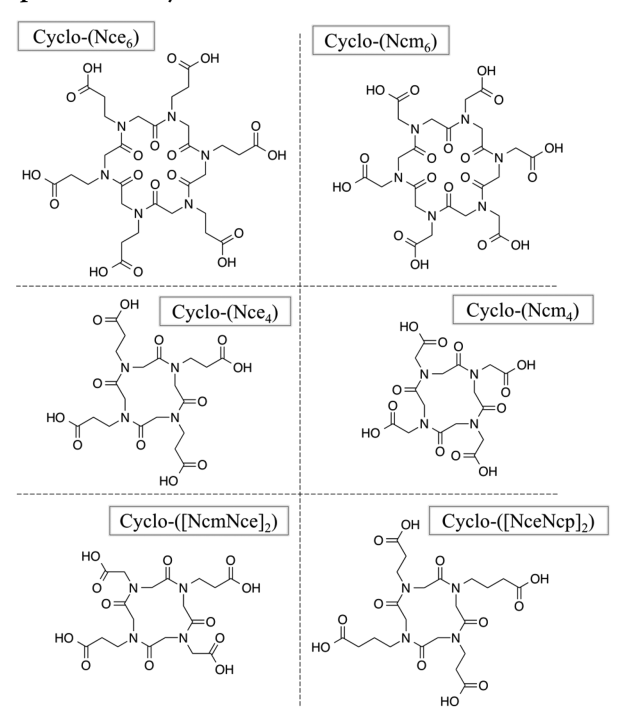
Typically, synthesis at a 0.28 mmol scale was conducted using 2-chlorotrityl chloride resin as the solid support to generate C-terminal carboxylic acid groups for the linear

Scheme 1. Chemical Structures and Atom Descriptors of Peptoid Monomers Used in This  $\operatorname{Work}^a$ 

"(A) Ncm, N-(carboxymethyl)glycine; (B) Nce, N-(carboxyethyl)glycine; and (C) Ncp, N-(carboxyproyl)glycine. (D) Definitions of backbone and side chain dihedral angles for Nce residues. Residues are color-coded, and the subscripts in the atom descriptors indicate the residue number.

precursors. Following protocols we previously reported, the head-to-tail macrocyclization of the linear precursors was accomplished through intramolecular amide bond formation, which was assisted by PyBOP as a coupling reagent.<sup>36</sup> The solution-phase macrocyclization reactions were carried out in dry dichloromethane at a peptoid concentration of  $\sim 0.5$  mM. To the solution were added 6 equiv of diisopropylethylamine and 3 equiv of PyBOP to conduct the amide bond formation between the C- and N-termini. The cyclization reactions typically proceeded to completion after 14 h while stirring at 25 °C. The tert-butyl protecting groups were removed after the cyclized peptoid oligomers had been purified from the cyclization reaction mixtures. The chemical identities and purities of the final products were determined by electrospray ionization mass spectrometry (ESI-MS) and analytical highperformance liquid chromatography (HPLC), respectively (see the Supporting Information for details). The six macrocyclic peptoid products were obtained in the form of polyprotic acids (Scheme 2). The introduction of cationic

Scheme 2. Chemical Structures and Descriptors of the Six Peptoid Macrocycles Studied in This Work<sup>a</sup>



<sup>a</sup>The macrocycles incorporate a carboxylic acid group within each of the oligomer side chains.

metal counterions and the full deprotonation of the carboxylic acid groups were achieved by directly dissolving the lyophilized cyclopeptoid powders in an aqueous NaOH or KOH solution to obtain a pH  $\sim$ 7.5. Diffraction-quality single crystals were obtained from the corresponding aqueous solutions by slow solvent evaporation.

X-ray Crystallographic Studies. Peptoid Cyclohexamers. We initiated our study by investigating the metal complexation of two cyclohexapeptoids (Scheme 2, top). Although hexameric peptoid macrocycles often show multiple isoenergetic backbone conformations in solution on the NMR time scale  $(10^{-2} \text{ s})$ , the addition of metal ions can promote the formation of a well-defined backbone con-

Crystal Growth & Design

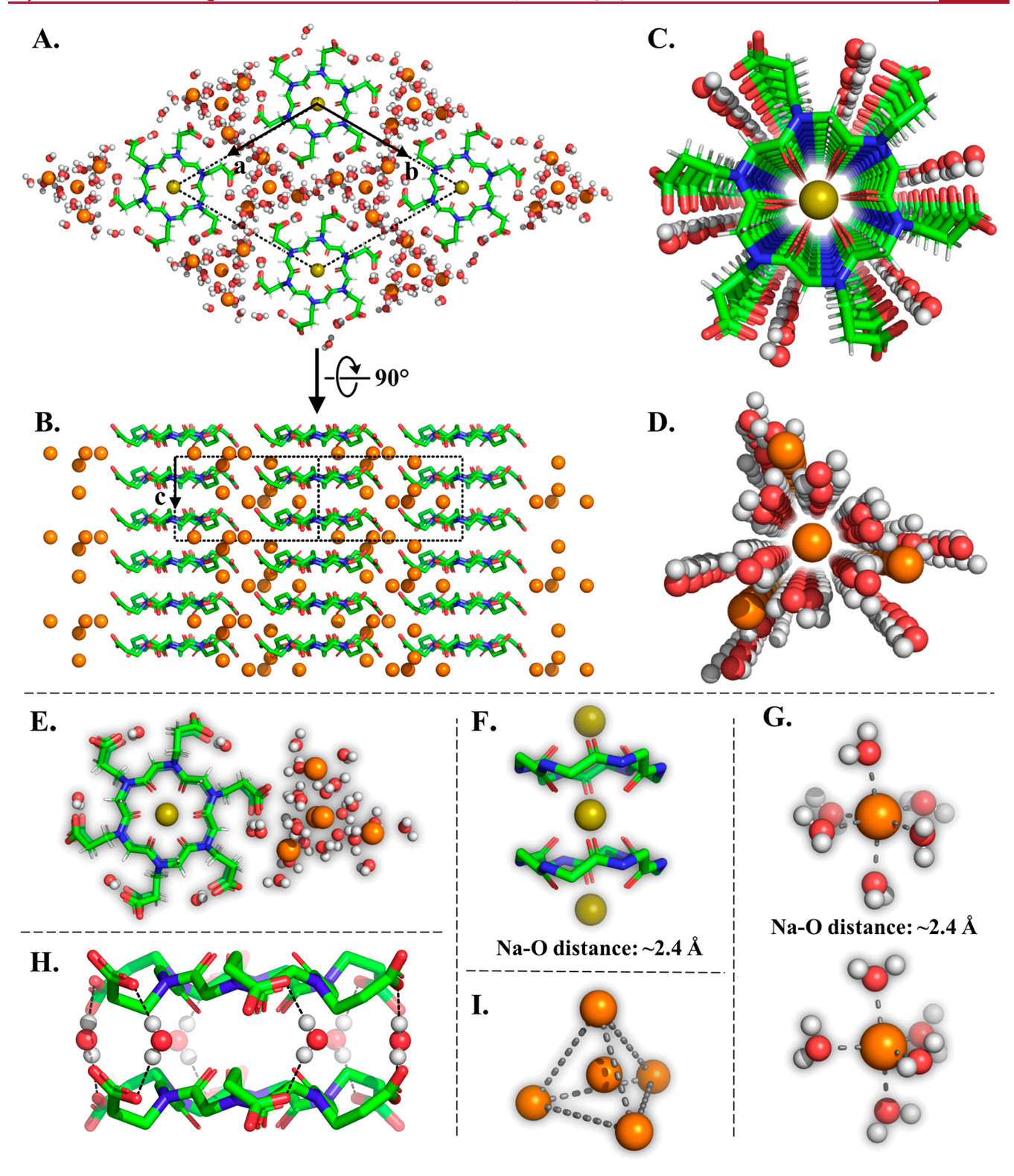


Figure 1. (A and B) Orthoscopic views of the X-ray crystal lattice structures formed by Cyclo-(Nce<sub>6</sub>)Na<sub>6</sub>(H<sub>2</sub>O)<sub>27</sub>. The unit cell is highlighted by dashed lines. In panel B, the hydrogen atoms, water molecules, and carbonyl-sodium ions are omitted for clarity. (C) Perspective view along the c-axis of the Na<sup>+</sup>-filled channels formed by Cyclo-(Nce<sub>6</sub>) peptoid macrocycles. (D) Perspective view of water channels that formed along the c-axis to accommodate the carboxylate-sodium ions. (E) Overview of the local Na–O coordination environment. (F) Coordination between carbonyl-sodium ions and backbone carbonyl oxygen atoms. (G) Coordination between carboxylate-sodium ions and oxygen atoms from water molecules. (H) Hydrogen bonds formed between water molecules and side chain carboxylate oxygen atoms, which are indicated by black dashed lines. (I) Tetrahedral sodium ion cluster. The tetrahedral geometry is indicated by gray dashed lines. Peptoid macrocycles are represented as sticks, and water molecules and sodium ions are represented by spheres. Color codes are as follows: light gray, hydrogen; green, carbon; blue, nitrogen; red, oxygen; orange, carboxylate-sodium ions; and olive, carbonyl-sodium ions.

Crystal Growth & Design pubs.acs.org/crystal

B.  $\begin{array}{c} \chi_1:-76.6^{\circ} \\ 90^{\circ} \\ \chi_1:-69.2^{\circ} \\ \chi_1:76.6^{\circ} \\ \end{array}$ Residue-4
Backbone RMSD: 0.29 A

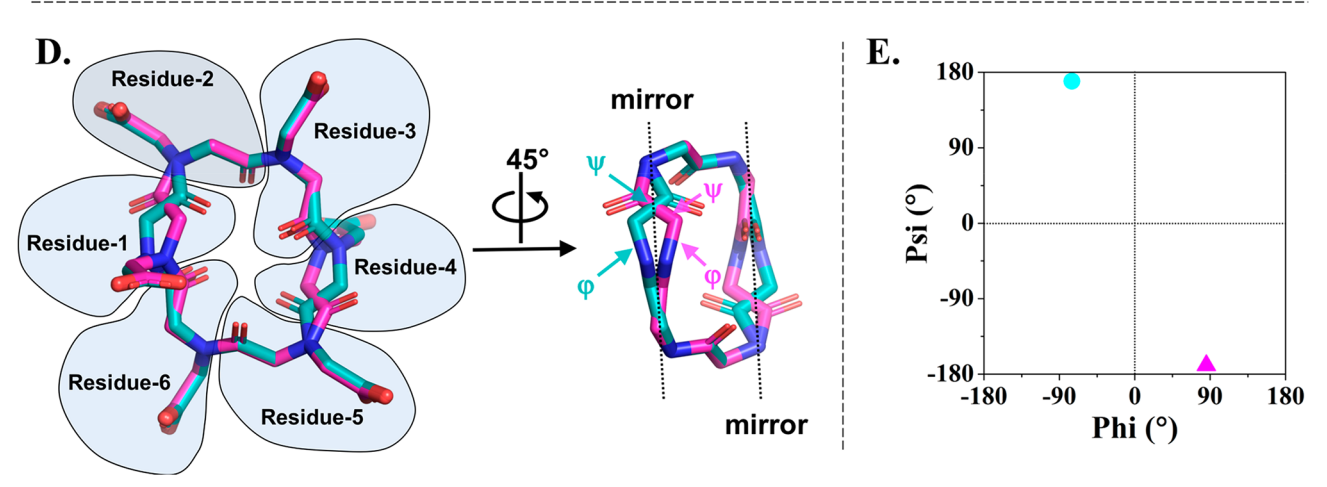


Figure 2. (A) Overview of the Cyclo-(Ncm<sub>6</sub>) peptoid macrocycle structure, which populates three different conformational states: type-I (100% occupancy), type-IIA (80% occupancy), and type-IIB (20% occupancy). (B) Orthoscopic views along the a-axis of the crystal lattice formed by Cyclo-(Ncm<sub>6</sub>)K<sub>6</sub>(H<sub>2</sub>O)<sub>13</sub>. The b-c-plane of the unit cells is indicated by the dashed lines. Hydrogen atoms, potassium ions, and water molecules are omitted for clarity. (C) Backbone superimposition between type-I and type-IIB Cyclo-(Ncm<sub>6</sub>) before and after a 90° rotation; only the side chains of residues 1 and 4 are shown, after rotation. (D) Structural comparison between type-IIA and type-IIB Cyclo-(Ncm<sub>6</sub>). Hydrogen atoms are omitted for clarity, and side chains are omitted after a 45° rotation. (E) Ramachandran plot of  $\phi$ - $\psi$  dihedral angles (as defined in panel D, right). Color codes for type-I, type-IIA, and type-IIB Cyclo-(Ncm<sub>6</sub>) are as follows: blue, nitrogen; red, oxygen; green, magenta; and cyan, carbon.

formation where all amide peptoid linkages are in the *trans*-geometry. <sup>35,54,55,61,65,69</sup> We hypothesized that with all *trans* backbone amide bonds, the presence of six side chain

carboxylate groups would induce an overall planar molecular geometry due to electrostatic repulsion between the negatively charged side chains. Furthermore, we considered how a combination of side chain—metal and backbone—metal interactions might propagate along orthogonal directions in the solid state, potentially resulting in the formation of metal-coordination-based supramolecular assemblies.

We were pleased to observe that, in the presence of  $Na^+$  and  $K^+$  ions,  $Cyclo-(Nce_6)$  and  $Cyclo-(Ncm_6)$  gave diffraction-quality crystals from the corresponding aqueous solutions. These two peptoid cyclohexamers crystallized with general formulas of  $Cyclo-(Nce_6)Na_6(H_2O)_{27}$  ( $P\overline{3}$  space group, Figure 1) and  $Cyclo-(Ncm_6)K_6(H_2O)_{13}$  ( $P\overline{1}$  space group, Figure 2), respectively.

Structure of Cyclo-(Nce<sub>6</sub>)Na<sub>6</sub>( $H_2O$ )<sub>27</sub>. Cyclo-(Nce<sub>6</sub>)<sup>55</sup> coassembled with sodium ions to form an unanticipated framework that included the presence of large hydrated channels. Based on the molecular formula determined by Xray crystallographic studies, 46% of the atoms in this crystal lattice were from water molecules. Cyclo-(Nce6) peptoid macrocycles stacked on one another, forming columnar tubular assemblies along the c-axis of the crystal lattice (Figure 1A and B). The interiors of these tubes were filled with Na+ ions. In addition, the peptoid columns were separated by groups of hydrated Na<sup>+</sup> ions. An analysis of the oligomer dihedral angles showed that each amide bond of Cyclo-(Nce<sub>6</sub>) was in the trans-conformation, and each residue adopted trans- $\alpha_D$  conformations with  $[\phi \sim 73^{\circ}, \psi]$  $\sim 176^{\circ}$ ] or  $[\phi \sim 287^{\circ}, \psi \sim 184^{\circ}]$  (Figure S15 and Table S10).<sup>70</sup> This motif is consistent with the CPM<sub>1</sub>'/CPM loops previously described for metalated hexameric cyclic peptoids.<sup>35</sup> In addition, every other residue shares the same combination of backbone and side chain dihedral angles. As a result, Cyclo-(Nce<sub>6</sub>) peptoid macrocycles exhibited a C3 symmetry and a flat overall geometry.

The sodium ions that coassembled with Cyclo-(Nce<sub>6</sub>) could be classified into two types based on their different coordination environments. The first type, designated as carbonyl-sodium ions (represented by olive spheres in Figure 1), are those located inside the peptoid tubular assemblies that exclusively coordinate with backbone carbonyl oxygen atoms (Figure 1A, C, E, and F). Each carbonyl-sodium ion was located between two Cyclo-(Nce<sub>6</sub>) peptoid macrocycles and coordinated by six backbone carbonyl oxygen atoms, with Na-O distances of ~2.37 Å established by chargedipole interactions. Three of the six backbone carbonyl oxygen atoms came from the peptoid macrocycle located above the carbonyl-sodium ion along c-axis and another three were from the macrocycle positioned below. Water-mediated hydrogen bonds between side chain carboxylate oxygen atoms were also found to facilitate the formation of peptoid tubular assemblies (Figure 1H), with donor-acceptor distances of  $2.8 \pm 0.1$  Å and hydrogen bond angles of

The second type of sodium ions was designated as carboxylate-sodium ions (represented by orange spheres in Figure 1), featuring unusual tetrahedral (edge length of  $5.9 \pm 0.2 \text{ Å}$ ) clusters of five sodium ions (Figure 1I). These sodium clusters are highly hydrated, and each carboxylate-sodium ion was coordinated by five or six water oxygen atoms with Na–O distances ~2.4 Å (Figure 1G, bottom and top, respectively). These water molecules formed channels along the *c*-axis of the crystal lattice to accommodate the carboxylate-sodium ions (Figure 1D). The minimum distance between any of these carboxylate-sodium ions and adjacent side chain carboxylate oxygen atoms was longer than 3.5 Å,

indicating that these hydrated and tetrahedral-shaped sodium clusters as a whole interacted with multiple adjacent side chain carboxylate groups from different Cyclo-(Nce<sub>6</sub>) peptoid macrocycles.

Structure of Cyclo- $(Ncm_6)K_6(H_2O)_{13}$ . Although the side chain flexibility decreased as we moved from Cyclo-(Nce<sub>6</sub>) to Cyclo-(Ncm<sub>6</sub>), the conformational heterogeneity of the Cyclo-(Ncm<sub>6</sub>) peptoid macrocycle increased, as Cyclo-(Ncm<sub>6</sub>) coassembled with potassium ions and water molecules in three different conformational states (Figure 2A and B). The unit cell of Cyclo- $(Ncm_6)K_6(H_2O)_{13}$ included type-I Cyclo-(Ncm<sub>6</sub>), which exhibited exclusively trans-amide (ttttt) geometries. The type-IIA conformation featured a unique and unprecedented cis-trans-trans-cistrans-trans (cttctt) amide bond sequence. 35,36,65,69 The type-IIB conformation exhibited all trans-amide geometries but included a different side chain orientation than that observed in the type-I conformational isomer (Figure 2C). An angle of  $\sim 80^{\circ}$  was found between the macrocyclic ring planes of the type-I and type-II conformers (Figure S7). The type-I conformer had a 100% occupancy in the unit cell, while the type-IIA and type-IIB conformers displayed 80% and 20% occupancies, respectively (Figure 2A and B). The backbone dihedral angles of all trans-amide residues were located in the predicted energy minima of the trans  $\alpha_D$  conformation, with  $[\phi \sim 77^{\circ}, \psi \sim 194^{\circ}] \text{ or } [\phi \sim 283^{\circ}, \psi \sim 166^{\circ}] \text{ (Figure S15)}$ and Table S9). The two cis-amide residues show backbone dihedral angles [ $\phi \sim 81^{\circ}$ ,  $\psi \sim 193^{\circ}$ ] or [ $\phi \sim 279^{\circ}$ ,  $\psi \sim$ 167°] and were located in the energy minima of the cis- $\alpha_{\rm D}$ conformation. These backbone conformational preferences also agree well with our previous QM calculations and are consistent with the  $\text{CP}_3'/\text{CP}_3$  cct  $\beta$ -turns described for hexameric cyclic peptoid models.

The most notable structural difference between the two alltrans-amide conformational isomers type-I and type-IIB Cyclo-(Ncm<sub>6</sub>) was the  $\chi_1$  dihedral angles in residues 1 and 4 (side chains were rotated by ~145°). Negligible differences were found when comparing the backbone conformations (RMSD value of 0.29 Å, Figure 2C). In contrast, the type-IIA and type-IIB conformations display almost coincident side chain positions but different backbone conformations. As shown in Figure 2D, the amide bond of residue 2 in the type IIA conformer was in the cis-geometry, while that in type IIB conformer was in the trans-geometry. Such a variation leads to a mirror-image relationship between the backbone dihedral  $\phi - \psi$  pair of residue 1 in the type IIA conformer and that in the type IIB conformer (Figure 2E). The same backbone conformational differences were also observed around residue 4 on the opposite side of the Cyclo-(Ncm<sub>6</sub>) macrocycle.

Ionic carboxylate—K<sup>+</sup> interactions dominate the solid-state assemblies of the Cyclo-(Ncm<sub>6</sub>) peptoid macrocycles. All potassium ions in this crystal lattice have a 100% occupancy and participated simultaneously in charge—charge and charge—dipole interactions. They were coordinated by either oxygen atoms from three different donors (water molecules, peptoid backbone amide groups, and side chain carboxylate groups) or oxygens from only water molecules and side chain carboxylate groups (Figures 3, S8, and S9, and Movie S1—S6). The K—O distances in these local interactions were ~2.75 Å, and the coordination numbers varied from five to seven. The conformational differences between the type-I and type II Cyclo-(Ncm<sub>6</sub>) peptoid macrocycles lead to variations in their potassium ion interactions. The most distinct

Crystal Growth & Design

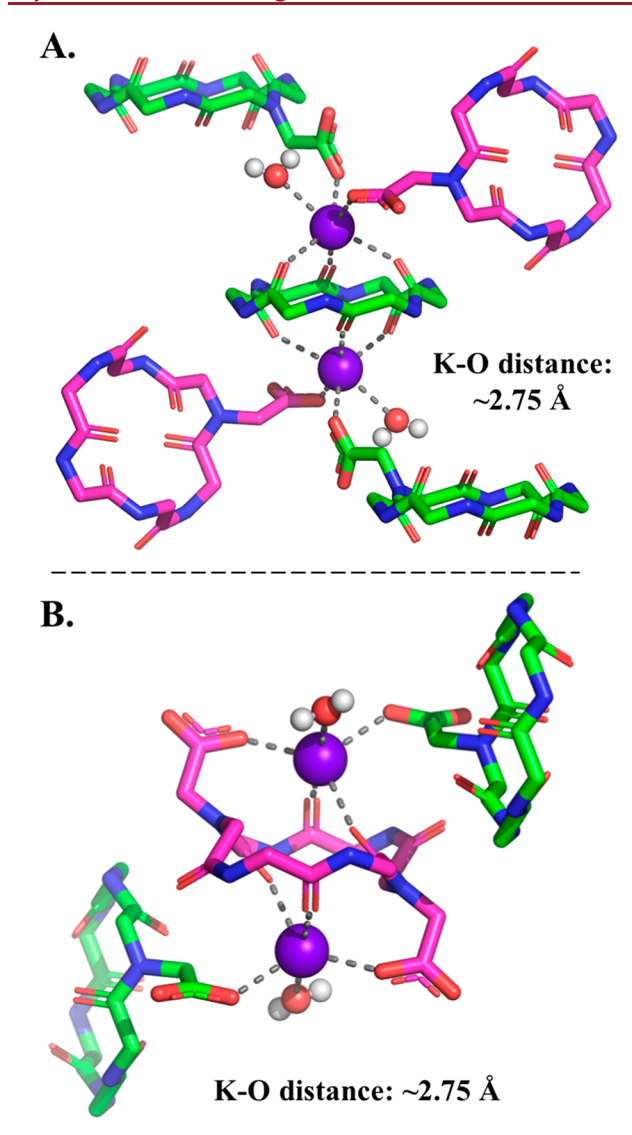


Figure 3. Examples of local K–O interactions observed in the crystal lattice formed by  $Cyclo\cdot(Ncm_6)K_6(H_2O)_{13}$ . The K–O coordination is highlighted by dashed gray lines. For clarity, hydrogen atoms are omitted for peptoid macrocycles, and only side chains that participate in K–O interactions are shown. Color codes are as follows: blue, nitrogen; red, oxygen; purple, potassium; green, carbon in type-I  $Cyclo\cdot(Ncm_6)$ ; and magenta, carbon in type-IIA  $Cyclo\cdot(Ncm_6)$ . See Figures S8 and S9 and Movies S1–S6 for other local K–O interactions.

difference is that the backbone carbonyl and side chain carboxylate oxygen atoms from the same **type-I** Cyclo-( $Ncm_6$ ) peptoid macrocycle were not able to coordinate with the same potassium ion (Figures 3 and S11), which was not the case for **type-II** Cyclo-( $Ncm_6$ ). Due to the different  $\chi_1$  side chain dihedral angles adopted by residue 1 and residue 4 in both **type-IIA** and **type-IIB** Cyclo-( $Ncm_6$ ) peptoid macrocycles, the side chain carboxylate oxygen atoms and backbone carbonyl atoms from the same peptoid macrocycle could interact with the same potassium ion. It is likely that this particular coordination mode with the potassium ions enables **type-IIA** Cyclo-( $Ncm_6$ ) peptoid macrocycles to adopt the unusual cttctt backbone amide sequence, which has not been previously observed.

Peptoid Cyclotetramers. We continued our study by varying the size of the peptoid macrocycle and investigating

the metal coassemblies formed by cyclic tetramers (Scheme 2, middle and bottom, respectively). Previous solution NMR studies showed that cyclotetrapeptoids possess a stable *cistrans-cis-trans* (ctct) backbone amide pattern, with a coalescence temperature >150 °C and  $\Delta G^{\ddagger} \sim 23$  kcal/mol. We hypothesized that the backbone of the cyclotetrapeptoids would retain this well-defined arrangement within the cyclotetrapeptoid—metal supramolecular assemblies and that variations of different peptoid side chains could play a critical role in determining the structural features of the resultant coassemblies.

The two cyclic homotetrameric peptoid oligomers, Cyclo- $(Nce_4)$  and  $Cyclo-(Ncm_4)$ , were both observed to coassemble with  $K^+$  cations (Figure 4). Cyclo- $(Nce_4)$  crystallized with  $K^+$  and water molecules in the *Pnma* space group with a formula of  $Cyclo-(Nce_4)K_4(H_2O)_7$  (Figure 4A). The  $Cyclo-(Ncm_4)$  macrocycles had shorter side chain lengths and crystallized as  $Cyclo-(Ncm_4)K_4(H_2O)_6$  within the  $P\overline{1}$  space group (Figure 4E).

We found that the two cyclic heterotetrameric peptoid oligomers were also able to coassemble with metal cations in hydrated environments. Cyclo-([NceNcp]<sub>2</sub>) and Cyclo-([NcmNce]<sub>2</sub>) were observed to crystallize in the  $P\overline{1}$  space group with the presence of  $K^+$  and  $Na^+$ , respectively (Figure 5). Cyclo-([NceNcp]<sub>2</sub>) crystallized with a formula of Cyclo-([NceNcp]<sub>2</sub>)  $K_4(H_2O)_9$  (Figure 5A), and Cyclo-([NcmNce]<sub>2</sub>) crystallized in a more hydrated state with a formula of Cyclo-([NcmNce]<sub>2</sub>) $Na_4(H_2O)_{14}$  (Figure 5E).

Only one molecular conformation was observed for all four of these cyclotetrapeptoids in the corresponding crystal lattice (Figure 6A-D), except for the slightly disordered side chain carboxylate groups of Cyclo-([NceNcp]<sub>2</sub>). As anticipated, these four cyclotetrapeptoids all adopted cis-trans-cis-trans (ctct) amide bond sequences. The backbone superimposition of these four cyclotetrapeptoids resulted in RMSD values below 0.10 Å (Figure 6E), indicating that they share the same backbone conformation despite the different side chain compositions. The peptoid monomers with trans-amide bonds show backbone dihedral angles  $[\phi \sim 130^{\circ}, \psi \sim$  $300^{\circ}$ ] or  $[\phi \sim 230^{\circ}, \psi \sim 60^{\circ}]$ , while the monomers with *cis*amide bonds show backbone dihedral angles  $[\phi \sim 98^{\circ}, \psi \sim$ 197°] or  $[\phi \sim 262^{\circ}, \psi \sim 163^{\circ}]$  (Tables S5–S8). In the Ramachandran-type plot, these backbone dihedral  $\phi$ - $\psi$  angle pairs are located in the energy minima of the trans- $C_{7\beta}$  and  $cis-\alpha_D$  conformations (Figure S15), respectively, as we previously predicted for a disarcosine model using quantum mechanical (QM) calculations. These values are also in accord with the  $CP_2$  and  $CP_2'$  tot  $\beta$ -turns described for tetrameric cyclic peptoid models. The second of the

Structures of Cyclo-(Nce<sub>4</sub>) $K_4(H_2O)_7$  and Cyclo-(Ncm<sub>4</sub>)- $K_4(H_2O)_6$ . Each of these two cyclotetrapeptoids formed parallel tubular assemblies by stacking along the *a*-axis of their crystal lattices (Figure 4A and E). The interior of the cylinders formed by Cyclo-(Ncm<sub>4</sub>) were empty and spatially isolated from the neighboring stacks (Figure 4E and F). In contrast, potassium ions were positioned inside the tubular assemblies formed by Cyclo-(Nce<sub>4</sub>) (Figure 4C). The K<sup>+</sup>-filled Cyclo-(Nce<sub>4</sub>) cylinders interpenetrated with their mirror-imaged counterparts along the *c*-axis to form layered structures (Figure 4A), which we refer to as a "peptoid—metal layer". Along the *b*-axis, these peptoid—metal layers were segregated by K<sup>+</sup>/H<sub>2</sub>O planes composed of potassium

Crystal Growth & Design pubs.acs.org/crystal Article

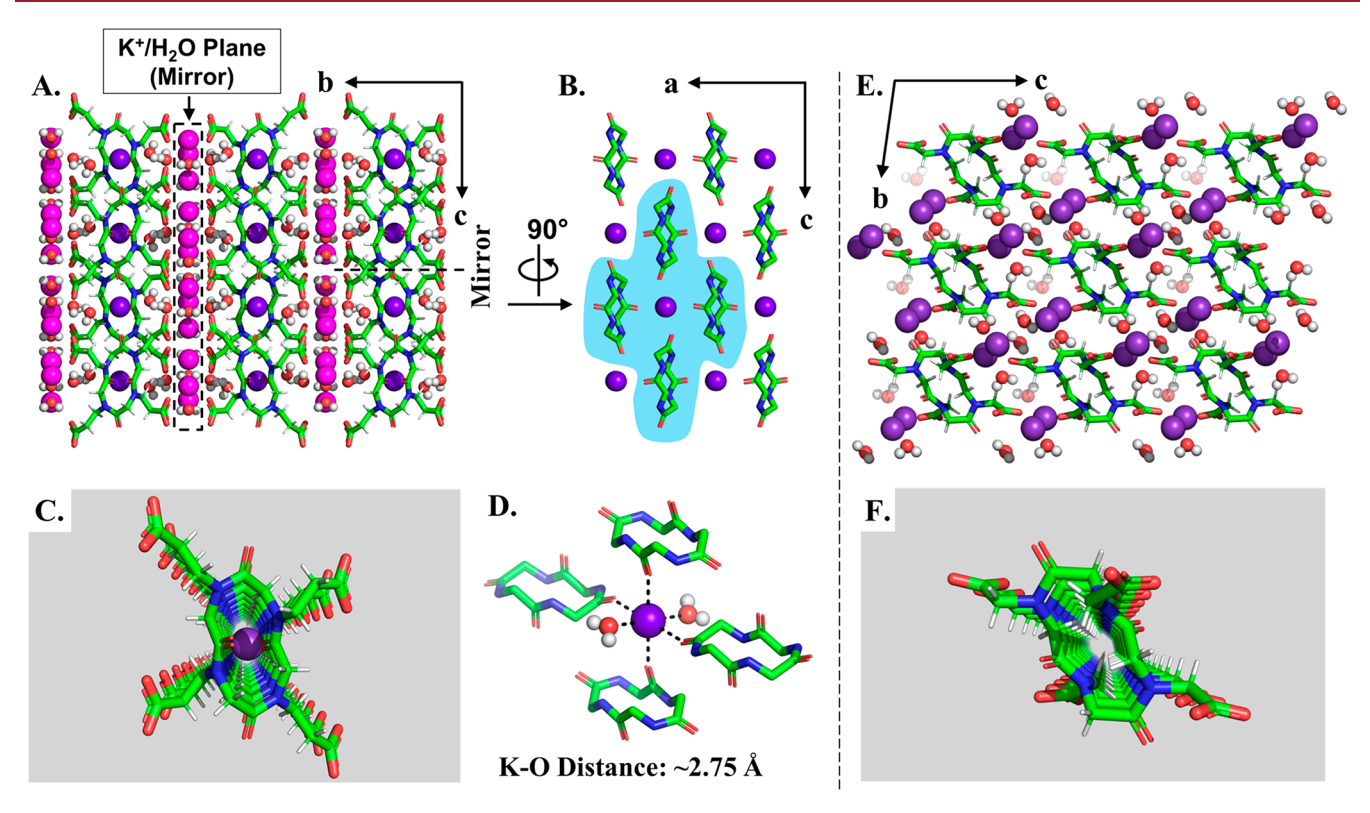


Figure 4. X-ray crystal structures of two homocyclotetrapeptoid—metal complexes. (A and B) Orthoscopic views of the crystal lattice structure formed by Cyclo-(Nce<sub>4</sub>)K<sub>4</sub>(H<sub>2</sub>O)<sub>7</sub>. For clarity, the side chains, carboxylate-potassium ions, and water molecules are omitted in panel B. (C) Perspective view along the *a*-axis of the K<sup>+</sup>-filled cylindrical stacks formed by Cyclo-(Nce<sub>4</sub>) peptoid macrocycles. (D) Detailed view of the charge—dipole interactions between carbonyl-potassium ions and coordinating oxygen atoms as highlighted in panel B. (E) Orthoscopic views along the *a*-axis of the crystal lattice structures formed by Cyclo-(Ncm<sub>4</sub>)K<sub>4</sub>(H<sub>2</sub>O)<sub>6</sub>. (F) Perspective views along the *a*-axis of the tubular structures formed by Cyclo-(Ncm<sub>4</sub>). Color codes are as follows: gray, hydrogen; green, carbon; blue, nitrogen; red, oxygen; purple and magenta, potassium. See Figures S10 and S11 for detailed views of other local K–O interactions.

ions and water molecules. The peptoid-metal layers show a specular arrangement across the  $K^+/H_2O$  planes.

Potassium ions in the crystal lattice of Cyclo-(Nce<sub>4</sub>)- $K_4(H_2O)_7$  formed a complex and elaborate coordination environment with neighboring oxygen atoms. These potassium ions could be unambiguously classified into two types based on their coordinating interactions. The first type, described as carbonyl-potassium ions (represented by purple spheres in Figure 4A-4D), were located within the tubular structures and participated in only charge-dipole interactions (Figure 4D). Each of these carbonyl-potassium ions was coordinated by four backbone carbonyl oxygen atoms and two water oxygen atoms, with K-O distances ~2.75 Å. Two interacting backbone carbonyl oxygen atoms were located on peptoid macrocycles positioned above and below the carbonyl-potassium ion along the a-axis, and another two oxygen atoms were located on peptoid macrocycles in the neighboring tubular structures along the c-axis (Figure 4B). The second type, designated as carboxylate-potassium ions (represented by magenta spheres in Figure 4A), were located within the K<sup>+</sup>/H<sub>2</sub>O planes. They interacted with oxygen atoms from both the carboxylate groups of the macrocycle side chain and water molecules through a combination of charge-charge and charge-dipole interactions, with K-O distances ~2.75 Å and a coordination number of six (Figure S11).

For  $Cyclo-(Ncm_4)K_4(H_2O)_6$ , all potassium ions interacted concurrently with oxygen atoms from the three different oxygen donors, forming networks of charge—dipole and

charge-charge interactions (Figure S10). The K-O distances were  $\sim$ 2.75 Å, and the potassium ions were all coordinated by six oxygen atoms.

Structures of Cyclo-([NceNcp]<sub>2</sub>)K<sub>4</sub>(H<sub>2</sub>O)<sub>9</sub> and Cyclo-([NcmNce]<sub>4</sub>)Na<sub>4</sub>(H<sub>2</sub>O)<sub>14</sub>. Similar to the two homocyclote-trapeptoids, parallel tubular assemblies were also formed by Cyclo-([NceNcp]<sub>2</sub>) and Cyclo-([NcmNce]<sub>2</sub>) stacking along the *a*-axis of their crystal lattices (Figure 5C and F, respectively).

Despite the different symmetry characteristics, the overall structure of the Cyclo-([NceNcp]<sub>2</sub>) $K_4(H_2O)_9$  crystal lattice was highly similar to that of Cyclo- $(Nce_4)K_4(H_2O)_7$  (Figures 4A-D and 5A-D). The interior of the cylinders formed by Cyclo-([NceNcp]<sub>2</sub>) was also occupied by potassium ions. These K+-filled Cyclo-[NceNcp]<sub>2</sub>) cylinders also interpenetrated with their mirror-imaged counterparts to form 'peptoid-metal layers", and these layers were also segregated by K<sup>+</sup>/H<sub>2</sub>O planes. A complex and elaborate coordination environment was also found for the potassium ions in this crystal lattice. The potassium ions in the crystal lattice of Cyclo-([NceNcp]<sub>2</sub>)K<sub>4</sub>(H<sub>2</sub>O)<sub>9</sub> could also be unambiguously classified as either carbonyl-potassium ions (represented by purple spheres in Figure 5A-D) or carboxylate-potassium ions (represented by magenta spheres in Figure 5A). Each carbonyl-potassium ion in this crystal lattice was coordinated by four backbone amide oxygen atoms and two water oxygen atoms, with K-O distances of ~2.75 Å (Figure 5D) identical to that of the carbonyl-potassium ion found in the crystal lattice of Cyclo- $(Nce_4)K_4(H_2O)_7$ . The carboxylate-potassium

Crystal Growth & Design pubs.acs.org/crystal Article

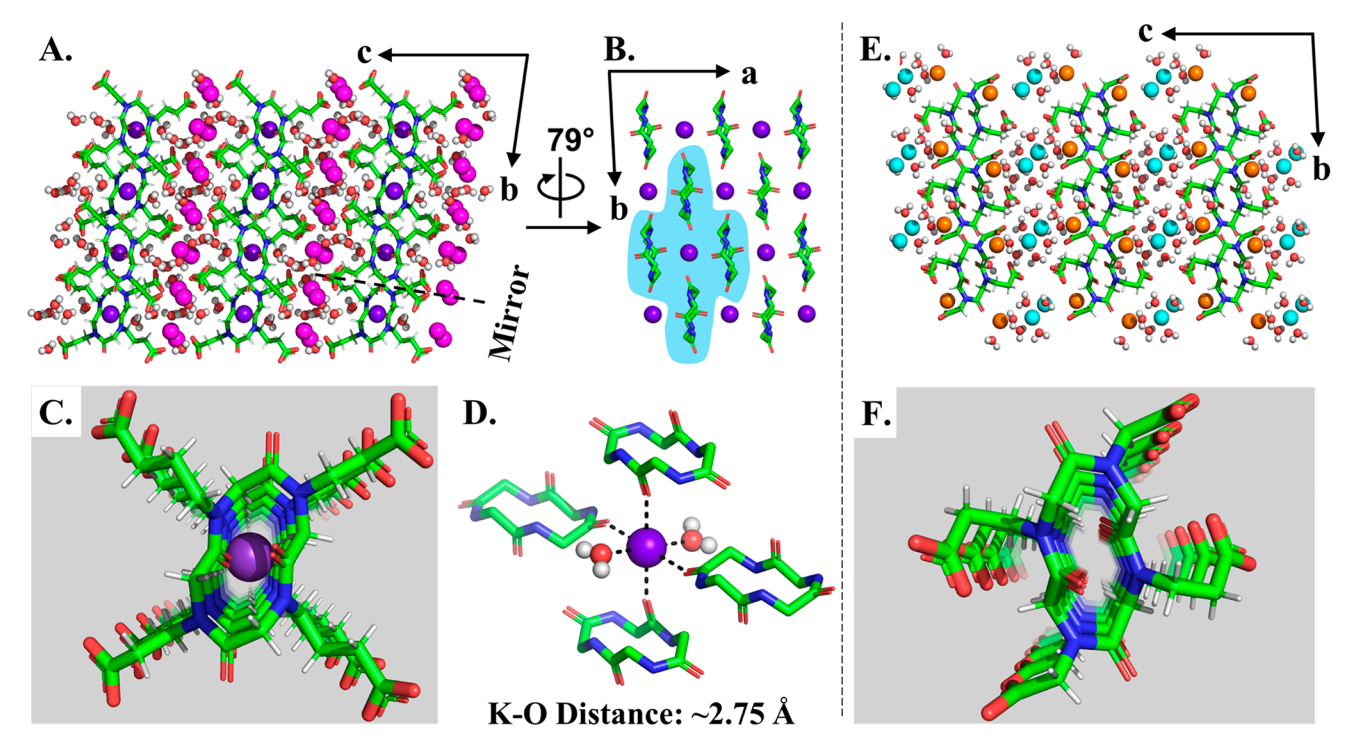


Figure 5. X-ray crystal structures of two heterocyclotetrapeptoid—metal complexes. (A and B) Orthoscopic views of the crystal lattice structure formed by Cyclo-([NceNcp]<sub>2</sub>)K<sub>4</sub>(H<sub>2</sub>O)<sub>9</sub>. In panel B, the side chains, carboxylate-potassium ions, and water molecules are omitted for clarity. (C) Perspective view along the *a*-axis of the K<sup>+</sup>-filled cylindrical stacks formed by Cyclo-([NceNcp]<sub>2</sub>) peptoid macrocycles. (D) Detailed view of the charge—dipole interactions between carbonyl-potassium ions and coordinating oxygen atoms, as highlighted in panel B. (E) Orthoscopic views along the *a*-axis of the crystal lattice structures formed by Cyclo-([NcmNce]<sub>2</sub>)Na<sub>4</sub>(H<sub>2</sub>O)<sub>14</sub>. (F) Perspective views along the *a*-axis of the tubular structures formed by Cyclo-([NcmNce]<sub>2</sub>). Color codes are as follows: gray, hydrogen; blue, nitrogen; red, oxygen; green, carbon; purple, carbonyl-potassium ion; magenta, carboxylate-potassium ion; and orange and cyan, sodium. See Figures S12 and S13 for other local metal—oxygen interactions.

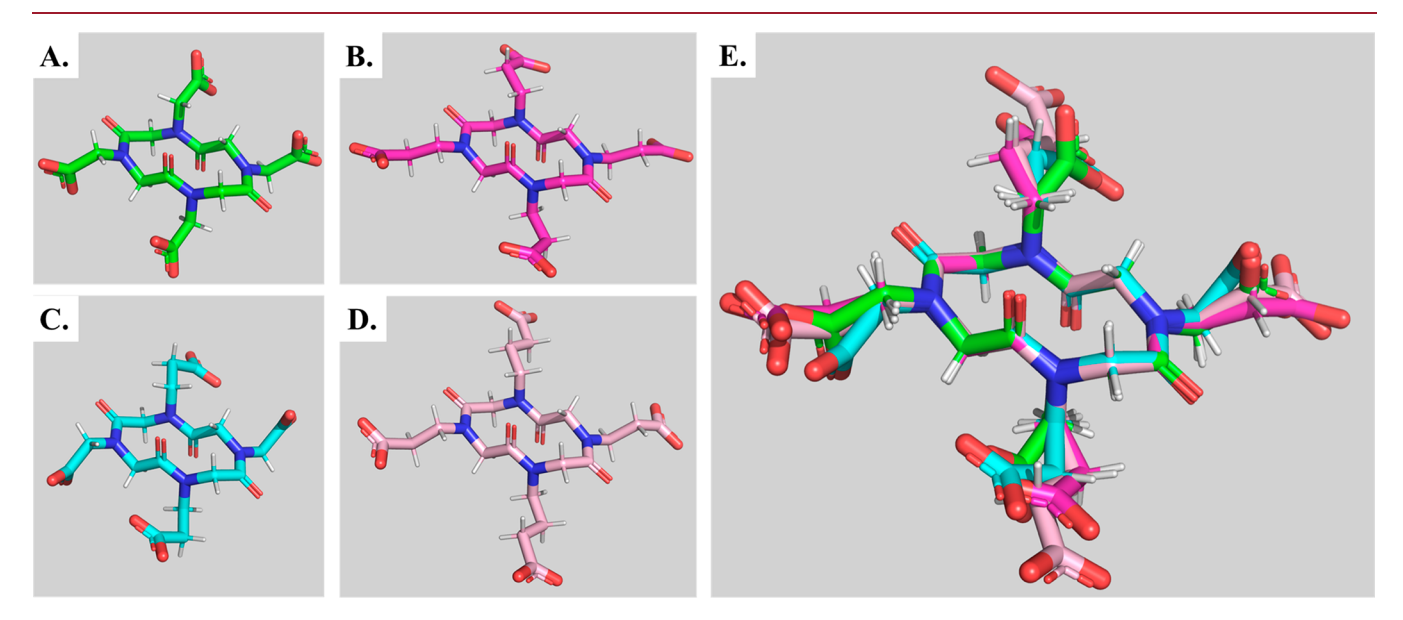


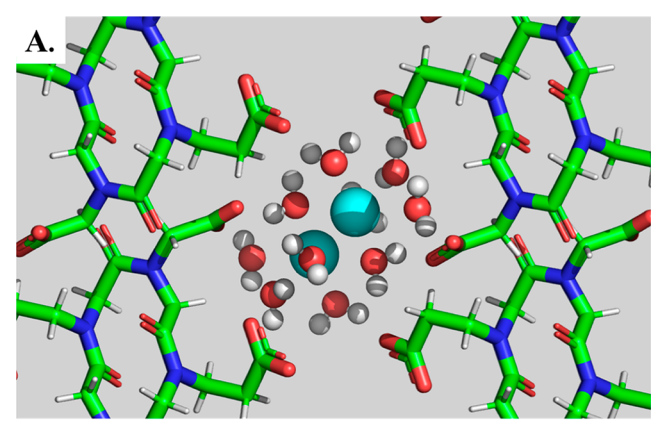
Figure 6. Comparison of X-ray crystal structures of the four cyclotetrapeptoids: (A) Cyclo-(Ncm<sub>4</sub>), (B) Cyclo-(Nce<sub>4</sub>), (C) Cyclo-([NcmNce]<sub>2</sub>), and (D) Cyclo-([NceNcp]<sub>2</sub>). (E) Superimpositions of the backbone atoms from the four cyclotetrapeptoids (backbone RMSD <0.10 Å). Color codes are as follows: light gray, hydrogen; blue, nitrogen; red, oxygen; green, Cyclo-(Ncm<sub>4</sub>) carbons; magenta, Cyclo-(Nce<sub>4</sub>) carbons; cyan, Cyclo-([NcmNce]<sub>2</sub>) carbons; and pink, Cyclo-([NceNcp]<sub>2</sub>) carbons.

ions concurrently participated in charge—dipole and charge—charge interactions, with K–O distances of  $\sim$ 2.79 Å and a coordination number of seven (Figure S13).

In contrast, the interior of the cylinders formed by Cyclo-([NcmNce]<sub>2</sub>) was empty, as observed for Cyclo-(Ncm<sub>4</sub>)

(Figures 4E and F and 5E and F). Sodium ions in the crystal lattice of  $Cyclo-([NcmNce]_2)Na_4(H_2O)_{14}$  were coordinated by the neighboring oxygen atoms in two different ways. Similar to the carboxylate-sodium ions observed for  $Cyclo-(Nce_6)Na_6(H_2O)_{27}$ , the sodium ions represented by cyan

spheres in Figure 5E were also named carboxylate-sodium ions. Pairs of these carboxylate-sodium ions formed diatomic clusters in a hydrated environment, with Na–Na distances of 3.5 Å (Figure 7A). Each carboxylate-sodium ion was solely



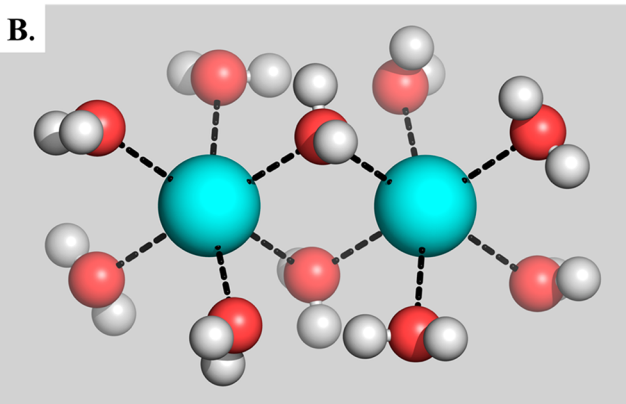


Figure 7. (A) Overview of the interactions between the hydrated diatomic cluster of sodium ions and neighboring side chain carboxylate groups from Cyclo-([NcmNce]<sub>2</sub>) peptoid macrocycles. (B) Detailed view of the coordination between water molecules and a diatomic cluster of sodium ions (Na–Na distance of 3.5 Å).

coordinated by oxygen atoms from water molecules, with Na–O distances of ~2.45 Å and a coordination number of six (Figure 7B). The distances between carboxylate-sodium ions and any adjacent carboxylate oxygen atoms were larger than 4.0 Å, suggesting that the diatomic sodium clusters interacted as a group with multiple neighboring side chain carboxylates. The sodium ions represented by orange spheres in Figure 5E simultaneously participated in charge—charge and charge—dipole interactions. They were found to concurrently coordinate with oxygen atoms from water molecules as well as backbone amide and side chain carboxylate groups (Figure S12). Each of these sodium ions was coordinated by five oxygen atoms, with Na–O distances of ~2.45 Å.

An analysis of the molecular conformations adopted by these two heterocyclotetrapeptoids revealed the length-dependent *cis*- or *trans*-amide bond preference of peptoid monomers that contain carboxylate side chains. The amide bonds of residues with shorter carboxylate side chains preferred to adopt the *cis*-conformation, while the amide bonds of monomers with longer side chains preferred the *trans*-conformation (Figure 5C and F, respectively).

## DISCUSSION

The complex frameworks formed by the co-assembly of the cyclopeptoid hexamer Cyclo-(Nce<sub>6</sub>), sodium ions, and water molecules are unprecedented. The Na+-filled channels formed by both water molecules and Cyclo-(Nce6) peptoid macrocycles create intriguing superstructures. The Na+-filled Cyclo-(Nce6) tubular assemblies found in this crystal lattice somewhat resemble ion channels observed in transmembrane proteins.<sup>72</sup> This tubular geometry is also similar to those of nanotubes self-assembled from cyclic peptides. 73,74 The interaction between the unusual hydrated Na<sup>+</sup> ion clusters and peptoid side chain carboxylate groups is an additional unusual feature that merits further investigation. The elaborate organization of Cyclo-(Nce<sub>6</sub>) peptoid macrocycles, sodium ions, and water molecules expands our peptoid design paradigms to include the possibility of additional unusual supramolecular frameworks.

To the best of our knowledge, the presence of the same small molecule in three different conformational forms in a crystallographic unit cell, as we found in the crystal lattice of  $Cyclo-(Ncm_6)K_6(H_2O)_{13}$ , is a rare observation in diffractometric studies of single crystals and unique in the peptoid field, as also established by the recent contribution from Tedesco et al. <sup>68,75–78</sup> This occurrence illustrates the conformational variety of cyclohexamer peptoids and their ability to afford unique solid-state assemblies.

The cis–trans–cis–trans (ctct) amide bond arrangement present in the carboxylic cyclotetrapeptoids reported in this work has also been consistently observed for other cyclotetrapeptoids, including cyclotetrasarcosine (oligo N-methyl glycines) and cyclotetrapeptoids bearing aromatic side chains, in both the solid state  $^{35,65-68}$  and solution. In addition to sharing the same amide bond sequence, all of these cyclotetrapeptoids share the same backbone conformation (backbone RMSD value below 0.2 Å, Figure S14). Taken together, the cis- $\alpha_{\rm D}$ –trans- $C_{7\beta}$ –cis- $\alpha_{\rm D}$ –trans- $C_{7\beta}$  backbone conformation is characteristic for this class of compounds.

Cyclo-(Ncm<sub>4</sub>), Cyclo-(Nce<sub>4</sub>), and Cyclo-([NceNcp]<sub>2</sub>) peptoid macrocycles all coassembled with potassium ions in hydrated environments. The structural differences of their crystal lattices strongly emphasize the important role played by the composition of peptoid side chains in determining the organization of resultant supramolecular assemblies.

The optimal arrangements of charge—charge and charge—dipole interactions are the key features of the six crystal lattice structures presented in this work. They are also the reason why diffraction-quality single crystals could be readily obtained from aqueous solutions. The metal-coordination parameters, the M–O distances (~2.4 Å for Na–O and ~2.8 Å for K–O), and coordination numbers (5–6 for Na $^+$  and 5–7 for K $^+$ ) found in this work are in good agreement with those determined for aqueous hydration structures and metalloprotein crystal structures that include Na $^+$  and K $^+$ .80–83

Previous studies have primarily focused on using metal coordination to control the conformation of individual peptoid macrocycles. <sup>24,35,53,55,61</sup> Our work significantly extends the influence of metal coordination to alter intermolecular interactions and thus enforce the unprecedented assembly of peptoid macrocycles within metal-coordinated supramolecular networks.

## CONCLUSION

In this work, we have demonstrated that peptoid macrocycles, both cyclotetrapeptoids and cyclohexapeptoids, are capable of co-assembling with cationic metal species to from structurally well-defined architectures. The formation of these coassemblies was driven by the combination of charge-dipole and charge-charge interactions. Oxygen atoms from water molecules, peptoid backbone amides, and side chain carboxylate groups all contributed to interactions with metal cations. The length of the side chains and the size of the macrocyclic rings were critical determinants of the organization between peptoid macrocycles and metal species in the solid state. In addition, the X-ray crystallographic data presented here (1) reinforce previous findings that cyclotetrapeptoids adopt a consistent rigid backbone conformation and thus may be considered "brick"-like building blocks for creating functional supramolecular assemblies and (2) establishes that the lack of hydrogen-bonding capabilities of the peptoid backbone does not limit the ability of peptoids to form ordered supramolecular assemblies.

The co-assembly strategy demonstrated in this work could be extended by varying both the cationic and anionic species to create a variety of ordered structures for a diverse range of applications, including electrolytes for high-performance solid-state batteries or bioactive metal—peptoid coassemblies. The conformations of both the peptoid backbone and the oligomer side chains can be tuned and are facilitated by the modular synthesis of these compounds, thus enabling the customized design and creation of co-assemblies with unique architectures and on-demand properties.

# ■ ASSOCIATED CONTENT

## Supporting Information

The Supporting Information is available free of charge at https://pubs.acs.org/doi/10.1021/acs.cgd.1c00209.

Materials, synthetic methods, crystal preparation and crystallographic methods, mass-spectrometry data, analytical HPLC traces, overview of the relative positions of peptoid macrocycles for type-I Cyclo-(Ncm<sub>6</sub>) and type-II Cyclo-(Ncm<sub>6</sub>), local view of metal—oxygen interactions, backbone conformational comparison between cyclotetrapeptoids, Ramachandran-type plots, crystal data, and torsion angles (PDF)

Local view of a different K–O coordination mode (MOV)

Local view of a different K-O coordination mode (MOV)

Local view of a different K-O coordination mode (MOV)

Local view of a different K–O coordination mode (MOV)

Local view of a different K-O coordination mode (MOV)

Local view of a different K–O coordination mode (MOV)

# **Accession Codes**

CCDC 2056722-2056727 contain the supplementary crystallographic data for this paper. These data can be obtained free of charge via www.ccdc.cam.ac.uk/data\_request/cif, or by emailing data\_request@ccdc.cam.ac.uk, or by contacting The Cambridge Crystallographic Data Centre,

12 Union Road, Cambridge CB2 1EZ, UK; fax: +44 1223 336033.

# AUTHOR INFORMATION

# **Corresponding Author**

Kent Kirshenbaum – Chemistry Department, New York University, New York 10003, United States; Email: kk54@ nyu.edu

#### **Authors**

Linhai Jiang — Chemistry Department, New York University, New York 10003, United States; o orcid.org/0000-0002-9403-9170

Chunhua Tony Hu − Chemistry Department, New York University, New York 10003, United States; ⑤ orcid.org/0000-0002-8172-2202

Francesco De Riccardis — Department of Chemistry and Biology "A. Zambelli", University of Salerno, 84084 Fisciano, Salerno, Italy; orcid.org/0000-0002-8121-9463

Complete contact information is available at: https://pubs.acs.org/10.1021/acs.cgd.1c00209

#### **Author Contributions**

L.J. and K.K. designed the research; L.J. conducted the syntheses and obtained peptoid crystals; C.T.H. determined the X-ray crystal structures; and L.J., F.D.R., and K.K. analyzed the results and wrote the manuscript. All authors have given approval to the final version of the manuscript.

#### Notes

The authors declare no competing financial interest.

## ACKNOWLEDGMENTS

This study was supported by award CHE-2002890 from the National Science Foundation (NSF). We acknowledge the contribution of the X-ray facility at NYU's Materials Research Science and Engineering Center (MRSEC) program under NSF Awards DMR-0820341 and DMR-1420073. Financial support (F.D.R.) was also received from the University of Salerno (FARB). We appreciate the generosity of Prof. Angelina Comotti at the Università degli Studi di Milano-Bicocca during discussions of our study and the guidance of Prof. Michael Ward at NYU. We acknowledge the contribution of James Eastwood and Brian Savino for assistance with this manuscript. We are grateful to the help from Xinyu Wang (Seeman Lab, NYU, NY, U.S.) at the early stage for determining the crystal structure of  ${\bf Cyclo-(Ncm_4)}$   ${\bf K_4(H_2O)_6}.$ 

#### ABBREVIATIONS

 $PyBOP, \ \ (benzotriazol-1-yloxy) tripyrrolidin ophosphonium hexafluorophosphate$ 

# **■** REFERENCES

- (1) Simon, R. J.; Kania, R. S.; Zuckermann, R. N.; Huebner, V. D.; Jewell, D. A.; Banville, S.; Ng, S.; Wang, L.; Rosenberg, S.; Marlowe, C. K. Peptoids: A Modular Approach to Drug Discovery. *Proc. Natl. Acad. Sci. U. S. A.* **1992**, *89*, 9367–9371.
- (2) Culf, A. S. Peptoids as Tools and Sensors. *Biopolymers* 2019, 110, No. e23285.
- (3) Kirshenbaum, K.; Barron, A. E.; Goldsmith, R. A.; Armand, P.; Bradley, E. K.; Truong, K. T. V.; Dill, K. A.; Cohen, F. E.; Zuckermann, R. N. Sequence-Specific Polypeptoids: A Diverse

- Family of Heteropolymers with Stable Secondary Structure. *Proc. Natl. Acad. Sci. U. S. A.* **1998**, 95, 4303–4308.
- (4) Sun, J.; Zuckermann, R. N. Peptoid Polymers: A Highly Designable Bioinspired Material. *ACS Nano* **2013**, *7*, 4715–4732.
- (5) Burkoth, T. S.; Beausoleil, E.; Kaur, S.; Tang, D.; Cohen, F. E.; Zuckermann, R. N. Toward the Synthesis of Artificial Proteins: The Discovery of an Amphiphilic Helical Peptoid Assembly. *Chem. Biol.* **2002**, *9*, 647–654.
- (6) Kirshenbaum, K.; Zuckermann, R. N.; Dill, K. A. Designing Polymers That Mimic Biomolecules. *Curr. Opin. Struct. Biol.* **1999**, *9*, 530–535.
- (7) Chongsiriwatana, N. P.; Patch, J. A.; Czyzewski, A. M.; Dohm, M. T.; Ivankin, A.; Gidalevitz, D.; Zuckermann, R. N.; Barron, A. E. Peptoids that Mimic the Structure, Function, and Mechanism of Helical Antimicrobial Peptides. *Proc. Natl. Acad. Sci. U. S. A.* **2008**, *105*, 2794–2799.
- (8) Dohm, M. T.; Seurynck-Servoss, S. L.; Seo, J.; Zuckermann, R. N.; Barron, A. E. Close Mimicry of Lung Surfactant Protein B by "Clicked" Dimers of Helical, Cationic Peptoids. *Biopolymers* **2009**, 92, 538–553.
- (9) Huang, M. L.; Benson, M. A.; Shin, S. B. Y.; Torres, V. J.; Kirshenbaum, K. Amphiphilic Cyclic Peptoids That Exhibit Antimicrobial Activity by Disrupting Staphylococcus aureus Membranes. Eur. J. Org. Chem. 2013, 2013, 3560–3566.
- (10) Wang, Y.; Dehigaspitiya, D. C.; Levine, P. M.; Profit, A. A.; Haugbro, M.; Imberg-Kazdan, K.; Logan, S. K.; Kirshenbaum, K.; Garabedian, M. J. Multivalent Peptoid Conjugates Which Overcome Enzalutamide Resistance in Prostate Cancer Cells. *Cancer Res.* **2016**, 76, 5124–5132.
- (11) Schneider, J. A.; Craven, T. W.; Kasper, A. C.; Yun, C.; Haugbro, M.; Briggs, E. M.; Svetlov, V.; Nudler, E.; Knaut, H.; Bonneau, R.; Garabedian, M. J.; Kirshenbaum, K.; Logan, S. K. Design of Peptoid-Peptide Macrocycles to Inhibit the  $\beta$ -Catenin TCF Interaction in Prostate Cancer. *Nat. Commun.* **2018**, *9*, 4396.
- (12) Mukudai, S.; Kraja, I.; Bing, R.; Nalband, D. M.; Tatikola, M.; Hiwatashi, N.; Kirshenbaum, K.; Branski, R. C. Implementing Efficient Peptoid-Mediated Delivery of RNA-Based Therapeutics to the Vocal Folds. *Laryngoscope Investig. Otolaryngol.* **2019**, *4*, 640–644.
- (13) Patch, J. A.; Barron, A. E. Helical Peptoid Mimics of Magainin-2 Amide. J. Am. Chem. Soc. 2003, 125, 12092–12093.
- (14) Hara, T.; Durell, S. R.; Myers, M. C.; Appella, D. H. Probing the Structural Requirements of Peptoids That Inhibit HDM2-p53 Interactions. J. Am. Chem. Soc. 2006, 128, 1995–2004.
- (15) Czyzewski, A. M.; McCaig, L. M.; Dohm, M. T.; Broering, L. A.; Yao, L. J.; Brown, N. J.; Didwania, M. K.; Lin, J. S.; Lewis, J. F.; Veldhuizen, R.; Barron, A. E. Effective In Vivo Treatment of Acute Lung Injury with Helical, Amphipathic Peptoid Mimics of Pulmonary Surfactant Proteins. Sci. Rep. 2018, 8, 6795.
- (16) Huang, W.; Seo, J.; Willingham, S. B.; Czyzewski, A. M.; Gonzalgo, M. L.; Weissman, I. L.; Barron, A. E. Learning from Host-Defense Peptides: Cationic, Amphipathic Peptids with Potent Anticancer Activity. *PLoS One* **2014**, *9*, No. e90397.
- (17) Mojsoska, B.; Carretero, G.; Larsen, S.; Mateiu, R. V.; Jenssen, H. Peptoids Successfully Inhibit the Growth of Gram Negative E. coli Causing Substantial Membrane Damage. *Sci. Rep.* **2017**, *7*, 42332.
- (18) Green, R. M.; Bicker, K. L. Evaluation of Peptoid Mimics of Short, Lipophilic Peptide Antimicrobials. *Int. J. Antimicrob. Agents* **2020**, *56*, 106048.
- (19) Mojsoska, B.; Zuckermann, R. N.; Jenssen, H. Structure-Activity Relationship Study of Novel Peptoids That Mimic the Structure of Antimicrobial Peptides. *Antimicrob. Agents Chemother.* **2015**, *59*, 4112–4120.
- (20) Chongsiriwatana, N. P.; Miller, T. M.; Wetzler, M.; Vakulenko, S.; Karlsson, A. J.; Palecek, S. P.; Mobashery, S.; Barron, A. E. Short Alkylated Peptoid Mimics of Antimicrobial Lipopeptides. *Antimicrob. Agents Chemother.* **2011**, *55*, 417–420.

- (21) Stringer, J. R.; Crapster, J. A.; Guzei, I. A.; Blackwell, H. E. Extraordinarily Robust Polyproline Type I Peptoid Helices Generated via the Incorporation of  $\alpha$ -Chiral Aromatic N-1-Naphthylethyl Side Chains. *J. Am. Chem. Soc.* **2011**, *133*, 15559–15567.
- (22) Roy, O.; Dumonteil, G.; Faure, S.; Jouffret, L.; Kriznik, A.; Taillefumier, C. Homogeneous and Robust Polyproline Type I Helices from Peptoids with Nonaromatic  $\alpha$ -Chiral Side Chains. *J. Am. Chem. Soc.* **2017**, *139*, 13533–13540.
- (23) Gimenez, D.; Aguilar, J. A.; Bromley, E. H. C.; Cobb, S. L. Stabilising Peptoid Helices Using Non-Chiral Fluoroalkyl Monomers. *Angew. Chem., Int. Ed.* **2018**, *57*, 10549–10553.
- (24) Schettini, R.; Costabile, C.; Sala, G. D.; Iuliano, V.; Tedesco, C.; Izzo, I.; De Riccardis, F. Cation-Induced Molecular Switching Based on Reversible Modulation of Peptoid Conformational States. *J. Org. Chem.* **2018**, 83, 12648–12663.
- (25) Shah, N. H.; Butterfoss, G. L.; Nguyen, K.; Yoo, B.; Bonneau, R.; Rabenstein, D. L.; Kirshenbaum, K. Oligo(N-Aryl Glycines): A New Twist on Structured Peptoids. *J. Am. Chem. Soc.* **2008**, *130*, 16622–16632.
- (26) Wu, C. W.; Kirshenbaum, K.; Sanborn, T. J.; Patch, J. A.; Huang, K.; Dill, K. A.; Zuckermann, R. N.; Barron, A. E. Structural and Spectroscopic Studies of Peptoid Oligomers with α-Chiral Aliphatic Side Chains. *J. Am. Chem. Soc.* **2003**, *125*, 13525–13530.
- (27) Armand, P.; Kirshenbaum, K.; Goldsmith, R. A.; Farr-Jones, S.; Barron, A. E.; Truong, K. T. V.; Dill, K. A.; Mierke, D. F.; Cohen, F. E.; Zuckermann, R. N.; Bradley, E. K. NMR Determination of the Major Solution Conformation of a Peptoid Pentamer with Chiral Side Chains. *Proc. Natl. Acad. Sci. U. S. A.* 1998, 95, 4309–4314.
- (28) Armand, P.; Kirshenbaum, K.; Falicov, A.; Dunbrack, R. L.; Dill, K. A.; Zuckermann, R. N.; Cohen, F. E. Chiral N-Substituted Glycines Can Form Stable Helical Conformations. *Folding Des.* 1997, 2, 369–375.
- (29) Huang, K.; Wu, C. W.; Sanborn, T. J.; Patch, J. A.; Kirshenbaum, K.; Zuckermann, R. N.; Barron, A. E.; Radhakrishnan, I. A Threaded Loop Conformation Adopted by a Family of Peptoid Nonamers. *J. Am. Chem. Soc.* **2006**, *128*, 1733–1738.
- (30) Crapster, J. A.; Guzei, I. A.; Blackwell, H. E. A Peptoid Ribbon Secondary Structure. *Angew. Chem., Int. Ed.* **2013**, *52*, 5079–5084.
- (31) Wijaya, A. W.; Nguyen, A. I.; Roe, L. T.; Butterfoss, G. L.; Spencer, R. K.; Li, N. K.; Zuckermann, R. N. Cooperative Intramolecular Hydrogen Bonding Strongly Enforces cis-Peptoid Folding. J. Am. Chem. Soc. 2019, 141, 19436–19447.
- (32) Gorske, B. C.; Mumford, E. M.; Gerrity, C. G.; Ko, I. A Peptoid Square Helix via Synergistic Control of Backbone Dihedral Angles. *J. Am. Chem. Soc.* **2017**, *139*, 8070–8073.
- (33) Gorske, B. C.; Mumford, E. M.; Conry, R. R. Tandem Incorporation of Enantiomeric Residues Engenders Discrete Peptoid Structures. *Org. Lett.* **2016**, *18*, 2780–2783.
- (34) Mannige, R. V.; Haxton, T. K.; Proulx, C.; Robertson, E. J.; Battigelli, A.; Butterfoss, G. L.; Zuckermann, R. N.; Whitelam, S. Peptoid Nanosheets Exhibit a New Secondary-Structure Motif. *Nature* **2015**, *526*, 415–420.
- (35) D'Amato, A.; Pierri, G.; Tedesco, C.; Sala, G. D.; Izzo, I.; Costabile, C.; De Riccardis, F. Reverse Turn and Loop Secondary Structures in Stereodefined Cyclic Peptoid Scaffolds. *J. Org. Chem.* **2019**, *84*, 10911–10928.
- (36) Shin, S. B. Y.; Yoo, B.; Todaro, L. J.; Kirshenbaum, K. Cyclic Peptoids. J. Am. Chem. Soc. 2007, 129, 3218-3225.
- (37) Darapaneni, C. M.; Ghosh, P.; Ghosh, T.; Maayan, G. Unique beta-Turn Peptoid Structures and Their Application as Asymmetric Catalysts. *Chem. Eur. J.* **2020**, *26*, 9573–9579.
- (38) Ghadiri, M. R.; Soares, C.; Choi, C. A Convergent Approach to Protein Design. Metal Ion-Assisted Spontaneous Self-Assembly of a Polypeptide into a Triple-Helix Bundle Protein. *J. Am. Chem. Soc.* **1992**, *114*, 825–831.

- (39) Tunn, I.; de Léon, A. S.; Blank, K. G.; Harrington, M. J. Tuning Coiled Coil Stability with Histidine-Metal Coordination. *Nanoscale* **2018**, *10*, 22725–22729.
- (40) Barondeau, D. P.; Kassmann, C. J.; Bruns, C. K.; Tainer, J. A.; Getzoff, E. D. Nickel Superoxide Dismutase Structure and Mechanism. *Biochemistry* **2004**, *43*, 8038–8047.
- (41) Pyle, A. M. Ribozymes: A Distinct Class of Metalloenzymes. Science 1993, 261, 709-714.
- (42) Tikunova, S. B.; Liu, B.; Swindle, N.; Little, S. C.; Gomes, A. V.; Swartz, D. R.; Davis, J. P. Effect of Calcium-Sensitizing Mutations on Calcium Binding and Exchange with Troponin C in Increasingly Complex Biochemical Systems. *Biochemistry* **2010**, *49*, 1975–1984.
- (43) Kohn, W. D.; Kay, C. M.; Sykes, B. D.; Hodges, R. S. Metal Ion Induced Folding of a de Novo Designed Coiled-Coil Peptide. *J. Am. Chem. Soc.* **1998**, *120*, 1124–1132.
- (44) Lee, B.-C.; Chu, T. K.; Dill, K. A.; Zuckermann, R. N. Biomimetic Nanostructures: Creating a High-Affinity Zinc-Binding Site in a Folded Nonbiological Polymer. *J. Am. Chem. Soc.* **2008**, 130, 8847–8855.
- (45) Baskin, M.; Zhu, H.; Qu, Z.-W.; Chill, J. H.; Grimme, S.; Maayan, G. Folding of Unstructured Peptoids and Formation of Hetero-Bimetallic Peptoid Complexes upon Side-Chain-to-Metal Coordination. *Chem. Sci.* **2019**, *10*, 620–632.
- (46) Baskin, M.; Maayan, G. A Rationally Designed Metal-Binding Helical Peptoid for Selective Recognition Processes. *Chem. Sci.* **2016**, *7*, 2809–2820.
- (47) Maayan, G.; Ward, M. D.; Kirshenbaum, K. Metallopeptoids. Chem. Commun. 2009, 56–58.
- (48) Ghosh, T.; Fridman, N.; Kosa, M.; Maayan, G. Self-Assembled Cyclic Structures from Copper(II) Peptoids. *Angew. Chem.* **2018**, *130*, 7829–7834.
- (49) Zborovsky, L.; Smolyakova, A.; Baskin, M.; Maayan, G. A Pure Polyproline Type I-like Peptoid Helix by Metal Coordination. *Chem. Eur. J.* **2018**, 24, 1159–1167.
- (50) Baskin, M.; Panz, L.; Maayan, G. Versatile Ruthenium Complexes based on 2,2'-Bipyridine Modified Peptoids. *Chem. Commun.* **2016**, 52, 10350–10353.
- (51) Ghosh, P.; Fridman, N.; Maayan, G. From Distinct Metallopeptoids to Self-Assembled Supramolecular Architectures. *Chem. Eur. J.* **2021**, *27*, 634–640.
- (52) Zborovsky, L.; Tigger-Zaborov, H.; Maayan, G. Sequence and Structure of Peptoid Oligomers Can Tune the Photoluminescence of an Embedded Ruthenium Dye. *Chem. Eur. J.* **2019**, *25*, 9098–9107
- (53) Izzo, I.; Ianniello, G.; De Cola, C.; Nardone, B.; Erra, L.; Vaughan, G.; Tedesco, C.; De Riccardis, F. Structural Effects of Proline Substitution and Metal Binding on Hexameric Cyclic Peptoids. *Org. Lett.* **2013**, *15*, 598–601.
- ( $\tilde{5}4$ ) De Cola, C.; Licen, S.; Comegna, D.; Cafaro, E.; Bifulco, G.; Izzo, I.; Tecilla, P.; De Riccardis, F. Size-Dependent Cation Transport by Cyclic  $\alpha$ -Peptoid Ion Carriers. *Org. Biomol. Chem.* **2009**, 7, 2851–2854.
- (55) De Cola, C.; Fiorillo, G.; Meli, A.; Aime, S.; Gianolio, E.; Izzo, I.; De Riccardis, F. Gadolinium-Binding Cyclic Hexapeptoids: Synthesis and Relaxometric Properties. *Org. Biomol. Chem.* **2014**, *12*, 424–431.
- (56) Zuckermann, R. N.; Kerr, J. M.; Kent, S. B. H.; Moos, W. H. Efficient Method for the Preparation of Peptoids [Oligo(N-Substituted Glycines)] by Submonomer Solid-Phase Synthesis. *J. Am. Chem. Soc.* **1992**, *114*, 10646–10647.
- (57) Nguyen, A. I.; Spencer, R. K.; Anderson, C. L.; Zuckermann, R. N. A Bio-Inspired Approach to Ligand Design: Folding Single-Chain Peptoids to Chelate a Multimetallic Cluster. *Chem. Sci.* **2018**, 9, 8806–8813.
- (58) Knight, A. S.; Kulkarni, R. U.; Zhou, E. Y.; Franke, J. M.; Miller, E. W.; Francis, M. B. A Modular Platform to Develop Peptoid-based Selective Fluorescent Metal Sensors. *Chem. Commun.* **2017**, 53, 3477–3480.

- (59) Parker, B. F.; Knight, A. S.; Vukovic, S.; Arnold, J.; Francis, M. B. A Peptoid-Based Combinatorial and Computational Approach to Developing Ligands for Uranyl Sequestration from Seawater. *Ind. Eng. Chem. Res.* **2016**, *55*, 4187–4194.
- (60) Ricano, A.; Captain, I.; Carter, K. P.; Nell, B. P.; Deblonde, G. J.-P.; Abergel, R. J. Combinatorial Design of Multimeric Chelating Peptoids for Selective Metal Coordination. *Chem. Sci.* **2019**, *10*, 6834–6843.
- (61) Northrup, J.; Wiener, J.; Hurley, M.; Hou, C.-F. D.; Keller, T.; Baxter, R.; Zdilla, M. J.; Voelz, V.; Schafmeister, C. Metal-Binding Q-Proline Macrocycles. *J. Org. Chem.* **2021**, *86*, 4867–4876.
- (62) Nam, K. T.; Shelby, S. A.; Choi, P. H.; Marciel, A. B.; Chen, R.; Tan, L.; Chu, T. K.; Mesch, R. A.; Lee, B.-C.; Connolly, M. D.; Kisielowski, C.; Zuckermann, R. N. Free-Floating Ultrathin Two-Dimensional Crystals from Sequence-Specific Peptoid Polymers. *Nat. Mater.* **2010**, *9*, 454–460.
- (63) Robertson, E. J.; Olivier, G. K.; Qian, M.; Proulx, C.; Zuckermann, R. N.; Richmond, G. L. Assembly and Molecular Order of Two-Dimensional Peptoid Nanosheets through the Oil-Water Interface. *Proc. Natl. Acad. Sci. U. S. A.* **2014**, *111*, 13284–13289.
- (64) Battigelli, A.; Kim, J. H.; Dehigaspitiya, D. C.; Proulx, C.; Robertson, E. J.; Murray, D. J.; Rad, B.; Kirshenbaum, K.; Zuckermann, R. N. Glycosylated Peptoid Nanosheets as a Multivalent Scaffold for Protein Recognition. *ACS Nano* **2018**, *12*, 2455–2465.
- (65) Maulucci, N.; Izzo, I.; Bifulco, G.; Aliberti, A.; De Cola, C.; Comegna, D.; Gaeta, C.; Napolitano, A.; Pizza, C.; Tedesco, C.; Flot, D.; De Riccardis, F. Synthesis, Structures, and Properties of Nine-, Twelve-, and Eighteen-Membered N-Benzyloxyethyl Cyclic  $\alpha$ -Peptoids. *Chem. Commun.* **2008**, 3927–3929.
- (66) Groth, P. Crystal Structure of Cyclotetrasarcosyl. *Acta Chem. Scand.* **1970**, 24, 780–790.
- (67) Culf, A. S.; Čuperlović-Culf, M.; Léger, D. A.; Decken, A. Small Head-to-Tail Macrocyclic α-Peptoids. *Org. Lett.* **2014**, *16*, 2780–2783
- (68) Tedesco, C.; Erra, L.; Izzo, I.; De Riccardis, F. Solid State Assembly of Cyclic  $\alpha$ -Peptoids. CrystEngComm **2014**, 16, 3667–3687.
- (69) De Riccardis, F. The Challenge of Conformational Isomerism in Cyclic Peptoids. *Eur. J. Org. Chem.* **2020**, 2020, 2981–2994.
- (70) Butterfoss, G. L.; Renfrew, P. D.; Kuhlman, B.; Kirshenbaum, K.; Bonneau, R. A Preliminary Survey of the Peptoid Folding Landscape. *J. Am. Chem. Soc.* **2009**, *131*, 16798–16807.
- (71) Dale, J.; Titlestad, K. Conformational Processes in Simple Cyclic Peptides. *Acta Chem. Scand. Ser. B* **1975**, *29*, 353–361.
- (72) Öster, C.; Hendriks, K.; Kopec, W.; Chevelkov, V.; Shi, C.; Michl, D.; Lange, S.; Sun, H.; de Groot, B. L.; Lange, A. The Conduction Pathway of Potassium Channels is Water Free under Physiological Conditions. *Sci. Adv.* **2019**, *5*, No. eaaw6756.
- (73) Ghadiri, M. R.; Granja, J. R.; Milligan, R. A.; McRee, D. E.; Khazanovich, N. Self-Assembling Organic Nanotubes based on a Cyclic Peptide Architecture. *Nature* **1993**, *366*, 324–327.
- (74) Hartgerink, J. D.; Granja, J. R.; Milligan, R. A.; Ghadiri, M. R. Self-Assembling Peptide Nanotubes. *J. Am. Chem. Soc.* **1996**, *118*, 43–50.
- (75) Meli, A.; Macedi, E.; De Riccardis, F.; Smith, V. J.; Barbour, L. J.; Izzo, I.; Tedesco, C. Solid-State Conformational Flexibility at Work: Zipping and Unzipping within a Cyclic Peptoid Single Crystal. *Angew. Chem., Int. Ed.* **2016**, *55*, 4679–4682.
- (76) Pierri, G.; Landi, A.; Macedi, E.; Izzo, I.; De Riccardis, F.; Dinnebier, R. E.; Tedesco, C. Propyne Gas Adsorption in a Cyclic Hexapeptoid: A Combined In Situ XRPD and DFTB Study. *Chem. Eur. J.* **2020**, *26*, 14320–14323.
- (77) Pierri, G.; Schettini, R.; Nuss, J.; Dinnebier, R. E.; De Riccardis, F.; Izzo, I.; Tedesco, C. Cyclic Hexapeptoids with N-Alkyl Side Chains: Solid-state Assembly and Thermal Behaviour. *CrystEngComm* **2020**, *22*, 6371–6384.

Crystal Growth & Design

- (78) Pierri, G.; Corno, M.; Macedi, E.; Voccia, M.; Tedesco, C. Solid-State Conformational Flexibility at Work: Energetic Landscape of a Single Crystal-to-Single Crystal Transformation in a Cyclic Hexapeptoid. *Cryst. Growth Des.* **2021**, *21*, 897–907.
- (79) D'Amato, A.; Schettini, R.; Della Sala, G.; Costabile, C.; Tedesco, C.; Izzo, I.; De Riccardis, F. Conformational Isomerism in Cyclic Peptoids and Its Specification. *Org. Biomol. Chem.* **2017**, *15*, 9932–9942.
- (80) Mähler, J.; Persson, I. A Study of the Hydration of the Alkali Metal Ions in Aqueous Solution. *Inorg. Chem.* **2012**, *51*, 425–438.
- (81) Harding, M. M. Metal-Ligand Geometry Relevant to Proteins and in Proteins: Sodium and Potassium. *Acta Crystallogr., Sect. D: Biol. Crystallogr.* **2002**, *58*, 872–874.
- (82) Galib, M.; Baer, M. D.; Skinner, L. B.; Mundy, C. J.; Huthwelker, T.; Schenter, G. K.; Benmore, C. J.; Govind, N.; Fulton, J. L. Revisiting the Hydration Structure of Aqueous Na<sup>+</sup>. J. Chem. Phys. **2017**, 146, 084504.
- (83) Rowley, C. N.; Roux, B. The Solvation Structure of  $Na^+$  and  $K^+$  in Liquid Water Determined from High Level *ab Initio* Molecular Dynamics Simulations. *J. Chem. Theory Comput.* **2012**, 8, 3526–3535.